Geobiology

Geobiology (2013), **11**, 3–14 DOI: 10.1111/gbi.12018

A new look at saponite formation and its implications for early animal records in the Ediacaran of South China

J. HUANG,[1,2] X. CHU,[2,3] T. W. LYONS,[4] N. J. PLANAVSKY[4] AND H. WEN[5]

[1]*CAS Key Laboratory of Crust-Mantle Materials and Environments, School of Earth and Space Sciences, University of Science and Technology of China, Hefei, China*
[2]*State Key Laboratory of Lithospheric Evolution, Institute of Geology and Geophysics, Chinese Academy of Science, Beijing, China*
[3]*State Key Laboratory of Continental Dynamics, Northwest University, Xi'an, China*
[4]*Department of Earth Sciences, University of California, Riverside, CA, USA*
[5]*Institute of Geochemistry, Chinese Academy of Sciences, Guiyang, Guizhou, China*

ABSTRACT

Acanthomorphic acritarch fossils, including some interpreted to be the fossils of the earliest animal embryos, first appear in the lower Doushantuo Formation of the Yangtze Gorges area (YGA). Further, the complete paleontological and geochemical record for the YGA has played a central role in defining the global biological and geochemical backdrop that presaged and witnessed the dawn of diverse animal life. Despite the importance of the YGA in our understanding of Neoproterozoic Earth history, basic aspects about its depositional history remain debated. Foremost among the controversies, extensively studied sections in the YGA were recently tied to deposition in an alkaline lake, casting new but contentious light on the environments of early animal evolution and the broader significance of geochemical records from the YGA. Arguments for a lacustrine setting hinged on the presence of trioctahedral clays (saponite–corrensite). However, this clay type commonly forms in other environments, including the weathering profiles of mafic and ultramafic volcanics. Using a coupled geochemical and sedimentological approach, we argue that the trioctahedral clays in the lower Doushantuo of the YGA are better explained as weathering products from a regional mafic-to-ultramafic hinterland delivered by rivers to a shelf or lagoon in the Yangtze Gorges Basin. These novel provenance relationships for YGA sediments and associated clays are consistent with a marine setting for the early animal records and must factor in our current understanding of the broader geochemical fabric of the Doushantuo Formation.

Received 29 May 2012; accepted 17 October 2012

Corresponding author: X. Chu. Tel.: 86 10 82998417; fax: 86 10 62010846; e-mail: xlchu@mail.iggcas.ac.cn

INTRODUCTION

The Ediacaran Period (635–542 million years ago, Ma) is characterized by dramatic changes in Earth's geochemical cycles and high rates of biological diversification. These changes occurred in the aftermath of one of the most severe glacial episodes in Earth history (the 'Marinoan Snowball Earth Glaciation') (Hoffman & Schrag, 2002; Xiao, 2004). The appearance of new acanthomorphic acritarch fossils, some of which have been interpreted as early animal embryos or the resting stages of metazoa offspring, suggests metazoan diversification following glacial retreat (Xiao *et al.*, 1998; Yin *et al.*, 2007; Zhou *et al.*, 2007; Cohen *et al.*, 2009; McFadden *et al.*, 2009). Acanthomorphic acritarch fossils of possible metazoan origin first appear in the lower Doushantuo Formation of the Yangtze Gorges area (YGA). The first appearance of silicified acanthomorphic acritarchs occurs 6 m above the Nantuo cap carbonate in the Jiulongwan section, just above a 632.5 ± 0.5-Myr-old ash bed (Yin *et al.*, 2007). Recently, some fossils of the Doushantuo acanthomorphic acritarchs have also been explained as encysting protists classified as holozoans (Butterfield, 2011; Huldtgren *et al.*, 2011), but this placement remains uncertain (Huldtgren *et al.*, 2012;

Xiao *et al.*, 2012). The YGA is also unique among early Ediacaran locations for the combined strength of its geochemical record and accompanying prolific, diverse, and temporally varying fossils. This combination of data allows for the possibility of viewing early animal evolution in a strong environmental context. For example, the rocks of the YGA and age-equivalent strata in Oman provide our best archives of the remarkably depleted carbonate $\delta^{13}C$ values from this time period, which have been proposed to record the progressive ventilation of the Neoproterozoic ocean (Fike *et al.*, 2006; McFadden *et al.*, 2008).

Despite the important role the YGA has played in models for Ediacaran geobiology, its depositional setting remains debated, including widely disparate paleoenvironmental interpretations, making it difficult to grasp the full significance of the paleontological/geochemical record. Recently, for example, Bristow *et al.* (2009) suggested a non-marine depositional setting based principally on data from the YGA. The underlying argument for the non-marine hypothesis hangs on the ubiquitous presence of the clay mineral saponite in the lower part of Doushantuo Formation. Saponite typically forms in one of three settings: (i) alkaline, evaporative lakes [typically with pH > 9]; (ii) via weathering or very low-grade metamorphism of mafic and ultramafic rocks; and (iii) in association with hydrothermal alteration of volcanic rocks (Meunier, 2005; Velde & Meunier, 2008). Here, we use a coupled provenance and sedimentological approach to distinguish among the different modes of formation in our interpretation of saponite in the YGA. More specifically, we present several lines of evidence that point toward a detrital origin for the saponite formed from weathering of regional mafic–ultramafic rocks and transported to a restricted basin or a shelf lagoon (Jiang *et al.*, 2011), rather than autochthonous formation within a lake. Saponite in the YGA is found associated with sediments that, based on provenance tracers, derived from breakdown of mafic–to–ultramafic rocks, while the upper part of the formation, which lacks saponite, was sourced from a source terrain with an average shale composition.

GEOLOGICAL BACKGROUND AND SAMPLE DESCRIPTION

The Ediacaran in the YGA comprises the Doushantuo and Dengying formations, with alternating shale and carbonate rocks reaching a collective approximate thickness from <250 to 1000 m. The Doushantuo Formation spans most of the Ediacaran, which is constrained between 635 and 551 Ma (Condon *et al.*, 2005) (Fig. 1). The Doushantuo Formation in the YGA consists of 160–250 m of carbonate and black shale subdivided into four members. In the studied Jiulongwan section, the basal Member 1 is the 6-m-thick cap carbonate. The three submembers of Member 1 (C1, C2, and C3) have been well described in the YGA (Jiang *et al.*, 2003). Of relevance to our study, saponite has also been described from C1 and C3 in the YGA, including the Jiulongwan section (Bristow *et al.*, 2009). As much as 78 m of interbedded black shale and shaly limestone with abundant pea-sized chert and less-common phosphatic nodules overlies the cap carbonate in Member 2. Moving further up section, Member 3 consists of 58 m of medium- to thick-bedded dolostone intercalated with concretions and layers of chert (in the lower part) and thin-bedded marlstone (upper part). Member 4 consists of 14 m of thick black shale with scattered thin layers or lenses of dolomite (McFadden *et al.*, 2008) (Fig. 1).

Historically, the YGA has been viewed as an open marine, inner shelf setting during deposition of the

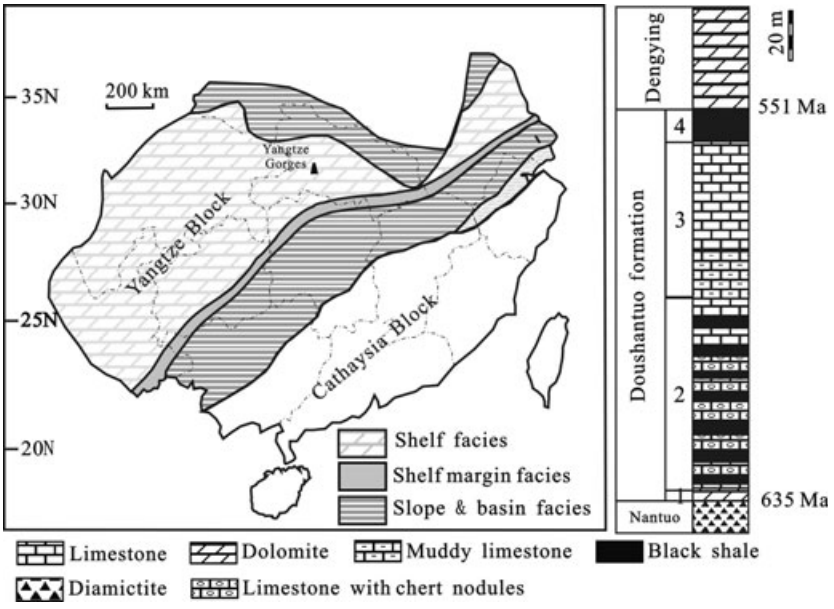

Fig. 1 Paleogeographic map and stratigraphic column of Doushantuo Formation, Jiulongwan section, Yangtze Gorges area.

Doushantuo Formation (Cao *et al.*, 1989). Vernhet (2007) further indicated that the Doushantuo Formation in this area accumulated in an intra-shelf basin—referred to here as the Yangtze Gorges Basin—which developed as a result of faulting and rapid transgression following the Nantuo (Marinoan) glaciation. It is difficult to ignore the possibility that Doushantuo sediments accumulated in a partially restricted setting in the early stage, but there is chemo-, litho-, and sequence-stratigraphic evidence supporting correlation of the Doushantuo Formation in the YGA with lower Ediacaran successions elsewhere in South China and distributed globally (McFadden *et al.*, 2008). Jiang *et al.* (2011) proposed that the Doushantuo Formation in the YGA was deposited on the shallow margin of a shelf lagoon. However, Bristow *et al.* (2009) argued for something radically different—a non-marine basin during the early Doushantuo stage, possibly unique from other basins in South China. To test this hypothesis and, more generally, explore the tectonic and depositional setting of the YGA, we have investigated the provenance of shales within the Doushantuo Formation.

ANALYTICAL METHODS

A total of 52 samples were collected for elemental analysis from Members 2, 3, and 4 of the Doushantuo Formation at the Jiulongwan section of the YGA. Stratigraphic locations for these samples are given in Table 1. Prior to chemical analysis, all the fresh samples were further trimmed to remove any weathered surfaces and ground to a powder (<200 mesh) using a tungsten carbide mill at the Institute of Geology and Geophysics, Chinese Academy of Sciences, Beijing.

About 50 mg of each sample powder was weighed and transferred to a Teflon bomb. Sample dissolution was carried out using a three acid (i.e., HNO_3, HF, and $HClO_4$) digest. The dissolved solutions were analyzed by ICP-MS at the Key Laboratory of Ore Deposit Geochemistry, Institute of Geochemistry, Chinese Academy of Sciences, Guiyang. Based on duplicate analysis of samples and geostandards, reproducibility was better than 92% for all of the analyzed trace metals and rare earth elements. Major element contents were analyzed on a Shimadzu X-Ray fluorescence spectrometer (XRF-1500) at State Key Laboratory of Lithospheric Evolution, Institute of Geology and Geophysics, Chinese Academy of Sciences, Beijing.

RESULTS AND DISCUSSION

Geochemical approaches to provenance

The total concentration of a given element in sediment can be subdivided into three independent fractions: detrital, biogenic, and hydrogenous (i.e., derived from seawater) (Piper, 1994). Different source terrains can have different detrital element compositions, which can be used to trace the provenance of the sediments (McLennan *et al.*, 1993). During weathering, most elements within source rocks, particularly Na, K, Ca, and Mg, are partially leached. In contrast, detrital elements (e.g., Al, Ti, Th, Hf, Sc and Zr) can be treated as essentially immobile elements because of the low solubility of their oxide and hydroxide phases in almost all low temperature aqueous solutions (McLennan & Taylor, 1991; Maynard, 1992; Nesbitt & Wilson, 1992; Ziemniak *et al.*, 1993). These elements have short residence times in seawater, and they can be transferred almost quantitatively to the sediment with little contribution from biogenic and hydrogenous processes. Therefore, these elements, such as Ti, Th, Zr, Sc, and Al, are used to denote the detrital fraction in shales (e.g., Böning *et al.*, 2004). However, some heavy minerals, such as zircon, monazite, and allanite, can be introduced during sedimentary sorting, which would elevate Zr, Hf, and Th concentrations in sediment. Fortunately, shales from the YGA show low Zr/Sc ratios (<10) and good correlations between Th/Sc and Zr/Sc (Fig. 2), which point away from later addition of Zr, Hf, and Th (McLennan *et al.*, 1990).

As a trace element indirectly sensitive to redox, Co might become authigenically enriched, although sediment Co abundance is more commonly tied to the abundance of clastic material (Tribovillard *et al.*, 2006). A strong correlation between Co and Al_2O_3 (Fig. 3) confirms the detrital origin for the Co and supports its availability as a provenance tracer.

Early diagenetic precipitation of phosphates can affect the rare earth element (REEs) chemistry of black shales enough to alter provenance signals (Lev *et al.*, 1999; Bright *et al.*, 2009). Although P_2O_5 contents are typically <0.3% in the analyzed Doushantuo Member 2 samples (Table 1), some samples do have higher P_2O_5 contents. Therefore, we have chosen not to use REEs as provenance tracers.

Provenance of the Doushantuo Formation

Figure 3 shows strong correlations among the concentrations of Co, Th, Zr, TiO_2, and Al_2O_3 in sedimentary rocks from the Doushantuo Formation but with two discrete trajectories in the cross-plots. Member 2 in the YGA shows a slope very different than those for Members 3 and 4, potentially suggesting fundamentally different sources, and these differences lie at the heart of our conclusions. Compared to Members 3 and 4, Member 2 has higher Co, Ti, and Zr and lower Th when normalized to Al content.

Ti/Al ratios support a mafic sediment source for Member 2 of the Doushantuo Formation. The Al in igneous rocks resides mostly in feldspars, while the Ti lies within mafic minerals (e.g., olivine, pyroxene, hornblende, biotite,

Table 1 Data for major and trace elements of sedimentary rocks of Doushantuo Formation

Sample#	JLW6.6	JLW7.75	JLW10.9	JLW11.74	JLW12.25	JLW13.0	JLW13.67	JLW15.37	JLW18.38	JLW18.90	JLW20.00	JLW21.86	JLW23.85
Depth(m)	6.60	7.75	10.90	11.74	12.25	13.00	13.67	15.37	18.38	18.90	20.00	21.86	23.85
Lithology	Shale	Shale	Shale	Shale	Shale	Shale	Shale	Shale	Shale	Shale	Shale	Shale	Shale
Member	Member 2	Member 2	Member 2	Member 2	Member 2	Member 2	Member 2	Member 2	Member 2	Member 2	Member 2	Member 2	Member 2
Sc	14.30	9.85	12.10	15.60	11.30	6.49	5.11	6.06	13.30	11.00	9.73	9.32	13.10
Co	19.70	14.80	16.90	23.70	15.80	9.98	9.87	9.94	19.90	16.20	17.70	13.80	17.70
Ge	1.54	0.78	1.00	1.18	0.89	0.57	0.54	0.52	1.23	0.96	0.90	0.80	1.00
Zr	133.00	76.40	106.00	134.00	94.10	46.80	35.20	55.00	117.00	95.00	82.10	81.50	120.00
La	132.00	16.20	15.80	19.00	10.70	15.80	8.04	15.70	39.40	18.50	27.10	10.90	13.80
Gd	20.16	3.15	3.11	4.17	2.15	2.64	1.48	2.20	7.44	3.89	4.17	2.24	3.46
Yb	3.69	1.32	1.70	2.12	1.27	0.84	0.63	0.81	2.70	1.90	1.41	1.24	1.63
Hf	3.27	1.83	2.66	3.18	2.47	1.26	0.86	1.40	2.87	2.36	1.99	2.02	2.91
Th	4.21	2.39	3.51	4.02	3.42	1.63	1.12	1.59	3.71	2.93	2.51	2.50	3.66
W	12.20	9.20	8.49	6.89	5.34	9.11	12.60	8.54	7.19	5.64	23.90	8.82	6.49
Zr/Sc	9.30	7.76	8.76	8.59	8.33	7.21	6.89	9.08	8.80	8.64	8.44	8.74	9.16
Th/Sc	0.29	0.24	0.29	0.26	0.30	0.25	0.22	0.26	0.28	0.27	0.26	0.27	0.28
SiO_2	33.59	31.45	52.68	45.69	44.94	38.90	36.61	34.38	40.70	44.35	39.80	31.36	40.22
TiO_2	1.11	0.61	0.87	1.20	0.77	0.37	0.29	0.42	1.03	0.80	0.68	0.70	0.98
Al_2O_3	8.85	5.17	7.41	9.02	6.91	3.23	2.52	3.15	7.67	6.55	5.71	5.38	8.34
$Fe_2O_3^T$	5.30	3.87	6.09	8.50	5.17	2.69	2.21	3.00	6.59	5.13	3.90	3.81	5.36
MnO	0.09	0.16	0.04	0.03	0.04	0.06	0.07	0.05	0.05	0.05	0.04	0.05	0.03
MgO	4.76	12.86	13.57	15.95	16.15	14.87	15.65	14.56	14.10	14.96	12.58	15.78	16.87
CaO	16.85	16.61	5.18	2.87	7.53	14.48	15.84	17.94	8.12	8.83	12.46	14.74	7.45
Na_2O	0.92	0.10	0.07	0.03	0.18	0.05	0.10	0.09	0.28	0.06	0.40	0.21	0.32
K_2O	3.15	1.46	0.88	1.15	0.50	0.28	0.09	0.16	1.36	0.96	1.46	1.15	2.27
P_2O_5	8.15	0.61	0.16	0.55	0.19	0.73	0.24	0.20	1.14	0.24	1.33	0.29	0.30
LOI	12.99	24.60	11.40	14.55	15.78	23.26	25.61	24.51	18.20	16.47	19.99	24.88	16.36
Total	95.76	97.50	98.35	99.54	98.16	98.92	99.23	98.46	99.24	98.40	98.35	98.35	98.50
Al_2O_3/TiO_2	7.97	8.48	8.52	7.52	8.97	8.73	8.69	7.50	7.45	8.19	8.40	7.69	8.51

Sample#	JLW26.23	JLW29.70	JLW31.13	JLW37.74	JLW39.72	JLW44.00	JLW48.80	JLW54.18	JLW59.10	JLW62.78	JLW64.70	JLW68.50	JLW72.3
Depth(m)	26.23	29.70	31.13	37.74	39.72	44.00	48.80	54.18	59.10	62.78	64.70	68.50	72.30
Lithology	Shale	Shale	Shale	Shale	Shale	Shale	Shale	Shale	Shale	Shale	Shale	Shale	Shale
Member	Member 2	Member 2	Member 2	Member 2	Member 2	Member 2	Member 2	Member 2	Member 2	Member 2	Member 2	Member 2	Member 2
Sc	9.81	9.35	4.19	7.88	7.50	8.83	9.14	6.69	5.01	8.08	6.13	8.78	5.41
Co	15.20	15.40	11.10	14.40	7.98	12.20	14.90	10.20	13.00	13.50	9.58	14.90	9.75
Ge	0.81	0.70	0.50	0.67	0.79	0.80	0.75	0.80	0.46	0.69	0.71	0.75	0.68
Zr	76.30	72.50	29.20	65.50	71.20	77.60	73.70	51.60	31.20	65.50	53.90	74.30	36.50
La	15.00	11.90	13.00	12.00	14.50	18.70	13.90	15.10	4.87	14.60	9.02	17.60	9.89
Gd	3.15	2.54	2.10	2.43	2.85	3.70	2.63	2.88	1.10	2.92	1.80	3.71	1.84
Yb	1.31	1.23	0.75	1.03	1.23	1.50	1.19	1.08	0.58	1.16	0.87	1.44	0.69
Hf	1.83	1.86	0.72	1.61	1.78	1.96	1.86	1.26	0.75	1.58	1.30	1.81	0.89
Th	2.57	2.13	1.00	2.20	2.42	2.59	2.21	1.92	1.11	2.31	1.71	2.75	1.33
W	8.10	4.72	15.30	13.90	5.51	6.01	8.13	5.62	11.10	5.45	13.70	12.90	13.20

Table 1 (continued)

Sample#	JLW26.23	JLW29.70	JLW31.13	JLW37.74	JLW39.72	JLW44.00	JLW48.80	JLW54.18	JLW59.10	JLW62.78	JLW64.70	JLW68.50	JLW72.3
Depth(m)	26.23	29.70	31.13	37.74	39.72	44.00	48.80	54.18	59.10	62.78	64.70	68.50	72.30
Lithology	Shale	Shale	Shale	Shale	Shale	Shale	Shale	Shale	Shale	Shale	Shale	Shale	Shale
Member	Member 2	Member 2	Member 2	Member 2	Member 2	Member 2	Member 2	Member 2	Member 2	Member 2	Member 2	Member 2	Member 2
Zr/Sc	7.78	7.75	6.97	8.31	9.49	8.79	8.06	7.71	6.23	8.11	8.79	8.46	6.75
Th/Sc	0.26	0.23	0.24	0.28	0.32	0.29	0.24	0.29	0.22	0.29	0.28	0.31	0.25
SiO_2	35.10	28.69	27.88	33.16	40.91	40.39	31.09	37.29	29.32	33.26	35.02	33.64	41.99
TiO_2	0.62	0.57	0.25	0.56	0.57	0.59	0.61	0.39	0.25	0.52	0.46	0.66	0.27
Al_2O_3	5.65	5.24	2.69	4.78	5.20	5.59	5.19	3.72	2.21	4.88	3.13	5.06	2.57
$Fe_2O_3^T$	4.00	3.70	1.93	4.04	3.17	3.46	3.56	2.79	2.17	3.60	1.99	3.10	2.29
MnO	0.03	0.04	0.03	0.03	0.02	0.03	0.04	0.02	0.04	0.03	0.02	0.02	0.03
MgO	16.72	17.59	17.87	15.58	13.58	14.41	17.09	16.06	17.29	16.38	15.29	15.11	13.85
CaO	11.91	14.67	18.06	13.67	12.16	11.79	13.40	13.70	18.16	13.85	15.53	14.16	14.32
Na_2O	0.21	0.05	0.07	0.22	0.26	0.25	0.06	0.34	0.09	0.01	0.16	0.03	0.21
K_2O	1.29	1.45	0.08	2.05	1.66	1.90	1.72	1.07	0.47	1.87	1.27	2.05	0.31
P_2O_5	0.33	0.25	0.60	0.50	0.53	0.81	0.33	1.43	0.12	0.73	0.68	1.83	0.48
LOI	22.53	25.85	29.96	23.44	22.30	21.41	24.32	22.35	29.86	23.49	25.76	22.62	23.23
Total	98.39	98.10	99.42	98.03	100.36	100.63	97.41	99.16	99.98	98.62	99.31	98.28	99.55
Al_2O_3/TiO_2	9.11	9.19	10.76	8.54	9.12	9.47	8.51	9.54	8.84	9.38	6.80	7.67	9.52

Sample#	JLW76.55	JLW78.0	JLW80.4	HND-1	HND-8	HND0.10	HND2.80	HND8.10	HND13.00	HND18.30	HND24.05	HND26.20	HND27.25
Depth(m)	76.55	78.00	80.40	90.00	92.00	115.10	117.80	123.10	128.00	133.30	139.05	141.20	142.25
Lithology	Shale	Shale	Shale	Limestone	Limestone	Limestone	Dolomite	Dolomite	Dolomite	Dolomite	Dolomite	Dolomite	Dolomite
Member	Member 2	Member 2	Member 2	Member 3	Member 3	Member 3	Member 3	Member 3	Member 3	Member 3	Member 3	Member 3	Member 3
Sc	8.58	5.76	7.21	3.35	2.88	6.45	5.18	4.51	4.99	2.34	2.68	2.45	2.63
Co	11.90	8.58	12.70	3.23	2.26	5.87	4.34	4.02	4.11	3.51	2.04	3.19	2.86
Ge	0.82	0.55	0.79	0.18	0.09	0.35	0.43	0.32	0.48	0.26	0.12	0.12	0.15
Zr	67.20	41.40	59.40	17.20	11.50	48.30	45.40	27.70	37.00	19.50	14.10	13.70	15.70
La	13.70	6.46	15.10	8.59	4.69	13.20	17.20	13.30	14.50	9.42	6.09	7.11	7.18
Gd	2.89	1.44	3.37	1.39	0.96	2.08	2.31	1.89	1.78	1.11	0.79	1.16	1.29
Yb	1.21	0.67	1.30	0.55	0.44	0.90	1.03	0.92	0.99	0.61	0.41	0.49	0.53
Hf	1.65	1.03	1.45	0.49	0.29	1.29	1.12	0.82	1.03	0.58	0.43	0.45	0.50
Th	2.39	1.50	2.14	2.69	1.82	4.80	5.87	4.38	5.60	3.21	2.22	2.23	2.39
W	4.82	5.89	8.71	0.50	0.72	1.11	1.17	0.76	0.90	0.53	0.57	0.47	0.49
Zr/Sc	7.83	7.19	8.24	5.13	3.99	7.49	8.76	6.14	7.41	8.33	5.26	5.59	5.97
Th/Sc	0.28	0.26	0.30	0.80	0.63	0.74	1.13	0.97	1.12	1.37	0.83	0.91	0.91
SiO_2	36.19	29.54	34.13	7.61	1.68	13.43	14.47	13.87	15.08	9.07	5.86	5.70	6.93
TiO_2	0.52	0.32	0.46	0.09	0.05	0.31	0.23	0.16	0.20	0.10	0.07	0.07	0.08
Al_2O_3	4.67	2.49	4.34	1.89	0.80	3.56	3.85	3.31	4.07	2.12	1.47	1.42	1.66
$Fe_2O_3^T$	3.48	2.13	3.20	0.75	0.75	1.50	1.99	1.31	1.35	0.86	0.50	1.14	0.62
MnO	0.03	0.03	0.03	0.02	0.04	0.03	0.04	0.02	0.02	0.01	0.01	0.01	0.01
MgO	16.78	18.57	18.53	4.08	21.57	17.89	16.96	2.12	2.64	1.03	0.83	0.75	2.00
CaO	12.47	17.04	13.12	44.52	29.51	24.02	24.17	40.95	38.86	46.34	49.23	48.92	46.99

Table 1 (continued)

Sample#	JLW76.55	JLW78.0	JLW80.4	HND-1	HND-8	HND0.10	HND2.80	HND8.10	HND13.00	HND18.30	HND24.05	HND26.20	HND27.25
Depth(m)	76.55	78.00	80.40	90.00	92.00	115.10	117.80	123.10	128.00	133.30	139.05	141.20	142.25
Lithology	Shale	Shale	Shale	Limestone	Limestone	Limestone	Dolomite	Dolomite	Dolomite	Dolomite	Dolomite	Dolomite	Dolomite
Member	Member 2	Member 2	Member 2	Member 3	Member 3	Member 3	Member 3	Member 3	Member 3	Member 3	Member 3	Member 3	Member 3
Na_2O	0.31	0.12	0.21	0.00	0.02	0.12	0.13	0.03	0.05	0.00	0.06	0.02	0.07
K_2O	1.78	0.71	1.31	0.67	0.10	1.85	1.60	1.77	2.18	1.01	0.51	0.52	0.55
P_2O_5	0.62	0.24	0.49	0.21	0.10	0.28	0.17	0.07	0.10	0.07	0.10	0.16	0.14
LOI	22.27	28.41	24.85	38.91	44.98	37.01	36.49	34.24	33.74	37.23	39.21	38.56	38.47
Total	99.12	99.60	100.67	98.75	99.60	100.00	100.10	97.85	98.29	97.84	97.85	97.27	97.52
Al_2O_3/TiO_2	8.98	7.78	9.43	21.00	16.00	11.48	16.74	20.69	20.35	21.20	21.00	20.29	20.75
Sample#	HND28.85	HND29.5	HND30.9	HND31.45	HND32.2	HND33.8	HND34.6	HND36.2	HND37.0	HND37.8	HND39.6	HND40.2	HND41.0
Depth (m)	143.85	144.50	145.90	146.45	147.20	148.80	149.60	151.20	150.00	152.80	153.60	155.20	156.00
Lithology	Shale	Shale	Shale	Shale	Shale	Shale	Shale	Shale	Shale	Shale	Shale	Shale	Shale
Member	Member 4	Member 4	Member 4	Member 4	Member 4	Member 4	Member 4	Member 4	Member 4	Member 4	Member 4	Member 4	Member 4
Sc	13.10	12.30	4.10	12.20	11.40	11.40	9.11	8.20	11.90	8.60	10.90	9.89	6.35
Co	12.20	12.30	2.04	10.70	12.30	11.00	9.16	9.27	10.90	9.57	13.40	11.20	8.31
Ge	1.53	2.53	0.25	1.42	1.21	1.34	0.96	0.98	1.52	0.85	1.12	0.97	0.50
Zr	113.00	102.00	13.50	99.90	106.00	94.20	82.70	77.50	96.80	70.40	94.10	86.90	61.30
La	30.80	39.60	23.00	41.80	36.30	34.10	35.70	24.10	42.80	23.50	28.60	35.60	23.40
Gd	3.68	6.09	2.33	9.10	4.78	4.87	5.74	2.23	8.30	3.82	4.16	4.68	3.10
Yb	2.34	3.06	2.23	3.53	2.60	2.47	2.25	1.63	3.42	2.02	2.17	2.62	1.62
Hf	3.12	2.66	0.36	2.76	2.84	2.53	2.32	2.17	2.51	1.56	2.42	2.95	2.09
Th	16.70	15.50	1.78	15.90	14.90	14.10	13.00	12.90	14.70	10.90	13.80	17.50	10.60
W	2.88	2.82	1.29	2.67	2.86	2.99	2.57	3.02	2.95	0.57	3.52	4.43	7.16
Zr/Sc	8.63	8.29	3.29	8.19	9.30	8.26	9.08	9.45	8.13	8.19	8.63	8.79	9.65
Th/Sc	1.27	1.26	0.43	1.30	1.31	1.24	1.43	1.57	1.24	1.27	1.27	1.77	1.67
SiO_2	60.89	58.25	10.90	56.62	58.77	61.44	62.98	60.88	55.06	65.63	60.17	46.55	30.48
TiO_2	0.61	0.58	0.07	0.55	0.60	0.52	0.47	0.45	0.54	0.46	0.54	0.47	0.35
Al_2O_3	12.88	12.27	1.33	11.33	12.49	10.88	9.87	9.20	11.10	9.41	10.85	9.40	6.14
$Fe_2O_3^T$	3.26	3.76	0.70	4.33	4.58	3.68	3.98	3.17	3.68	3.90	3.96	3.80	3.05
MnO	0.02	0.03	0.17	0.03	0.02	0.02	0.02	0.03	0.03	0.02	0.02	0.03	0.05
MgO	2.84	2.65	18.31	3.05	2.23	1.84	1.65	2.64	3.95	1.47	2.68	6.54	11.22
CaO	2.85	2.59	26.18	3.35	1.95	1.65	1.81	3.04	4.45	1.35	2.49	8.35	15.89
Na_2O	0.17	0.63	0.10	0.27	0.04	0.20	0.28	0.33	0.78	0.18	0.22	0.13	0.19
K_2O	6.30	6.44	0.60	5.37	5.88	5.27	4.88	4.44	4.96	4.28	4.67	3.98	2.60
P_2O_5	0.14	0.25	0.05	0.38	0.20	0.25	0.33	0.13	0.40	0.29	0.19	0.25	0.25
LOI	9.61	12.54	41.00	24.38	10.96	12.39	13.00	15.14	11.60	12.15	12.76	17.11	26.69
Total	99.57	99.99	99.41	109.66	97.72	98.14	99.27	99.45	96.55	99.14	98.55	96.61	96.91
Al_2O_3/TiO_2	21.11	21.16	19.00	20.60	20.82	20.92	21.00	20.44	20.56	20.46	20.09	20.00	17.54

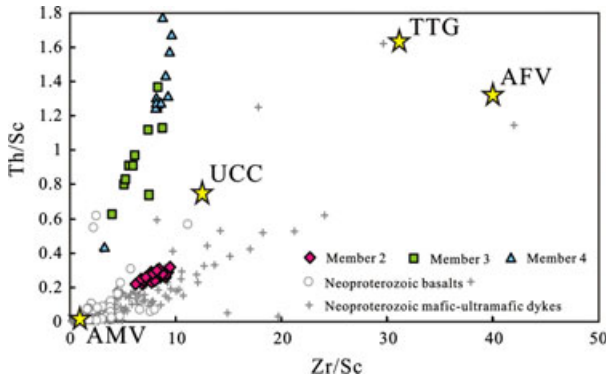

Fig. 2 Plot of Th/Sc vs. Zr/Sc for shales and carbonates of Doushantuo Formation. Full references for TTG (average of the Archean tonalite–trondhjemite–granodiorite series), UCC (average of the juvenile upper continental crust formed in interval of 2.5–1.8 Ga), AFV (average of the Archean felsic volcanics), AMV (average of the Archean mafic volcanic rocks). Data sources for Neoproterozoic basalts and mafic–ultramafic dykes are provided in the Supplementary Information.

and ilmenite). Thus, Al_2O_3/TiO_2 ratios can be useful as proxies for distinguishing among the different provenance relationships for sedimentary rocks (e.g., Hayashi *et al.*, 1997). Al_2O_3/TiO_2 ratios range from 3 to 8 for mafic igneous rocks, 8 to 21 for igneous rocks of intermediate composition, and 21 to 70 for felsic igneous rocks. Therefore, ratios of Al_2O_3 to TiO_2 for Member 2 ranging between 7 and 10 (Table 1) point to a dominantly mafic source. Similarly, as felsic rocks are enriched in Th and depleted in Zr, low Th/Al_2O_3 and high Zr/Al_2O_3 ratios in Member 2 argue for a significantly more mafic source terrain in the lower compared to the upper portion of the Doushantuo Formation.

Th/Sc ratios can also effectively fingerprint provenance relationships in sedimentary rocks, especially for igneous sources (McLennan *et al.*, 1993). Figure 2 shows the strong correlations between Th/Sc and Zr/Sc expressed in our data. However, the slope for Member 2 is much lower than that for Members 3 and 4. In Member 2, the Th/Sc-Zr/Sc relationship follows a trend spanning from average Archean mafic volcanic rocks (AMV) to average Archean felsic volcanics (AFV), suggesting inputs derived from discrete igneous sources. Furthermore, Th/Sc ratios are very low in Member 2 (<0.4) (Table 1), falling close to the ratio for AMV. McLennan *et al.* (1993) argued that very low sedimentary Th/Sc ratios (<1.0) are commonly an expression of mafic–ultramafic provenance. Data for Neoproterozoic mafic–ultramafic rocks on the Yangtze Block are plotted on Fig. 2, revealing a trend similar to that of Member 2 but with a larger range. Therefore, the sedimentary rocks in Member 2 can reasonably be attributed to a mafic-to-ultramafic source terrain. Th/Sc ratios in Members 3 and 4 are much higher than those for Member 2 (0.8–1.8) (Table 1) and suggest a common Th-rich provenance.

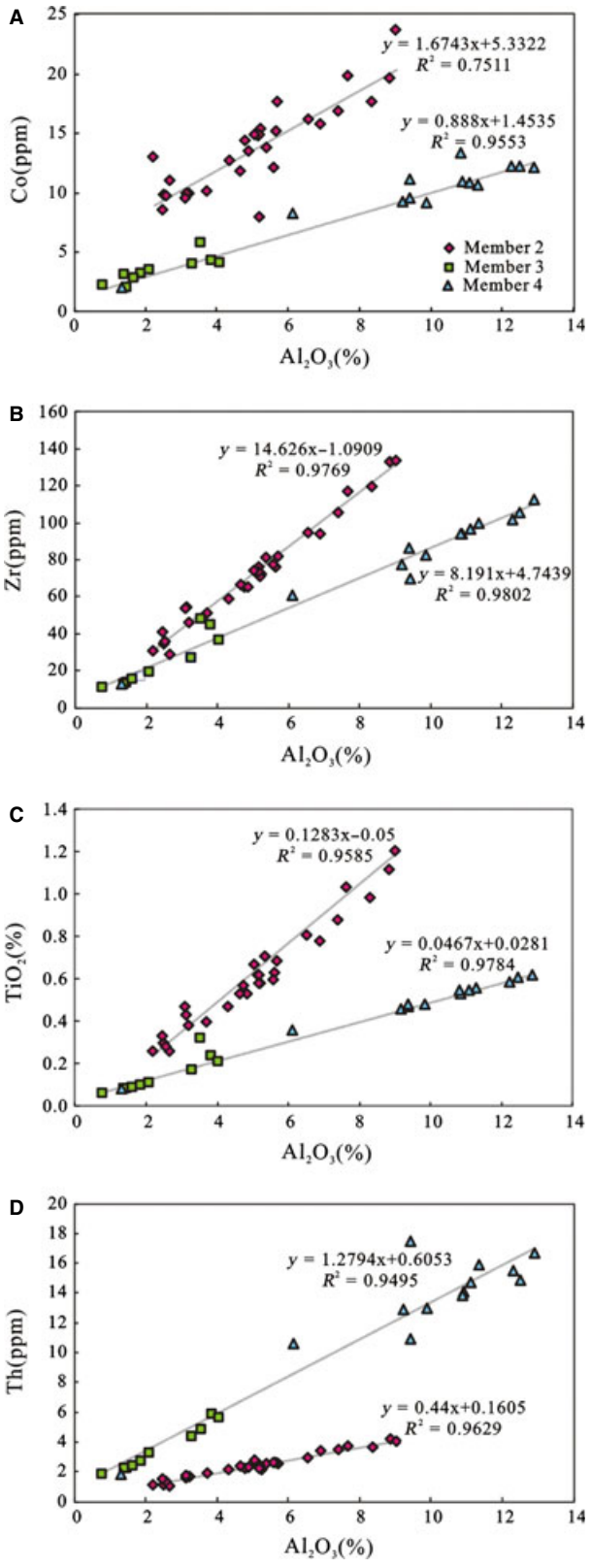

Fig. 3 Plots of Co vs. Al_2O_3 (A), Zr vs. Al_2O_3 (B), TiO_2 vs. Al_2O_3 (C), and Th vs. Al_2O_3 (D) for shales and carbonates of Doushantuo Formation.

Lastly, abundance of Th and Hf tracks felsic sources, whereas concentrations of Co reflect sources of mafic-to-ultramafic composition. Thus, Th–Hf–Co triangular plots are another tool available for distinguishing the provenance relationships of sedimentary rocks (Jahn & Condie, 1995). Data for Neoproterozoic mafic–ultramafic rocks on the Yangtze Block are also plotted on Fig. 4. In this figure, the data for Member 2 lie very close to the mafic–ultramafic zone, and the trend and range are also similar to those of Neoproterozoic mafic–ultramafic rocks on the Yangtze Block. In contrast, Members 3 and 4 fall in the field for Phanerozoic shales close to the values for PAAS (post-Archean Australian shale) and NASC (North American average shale) (Condie, 1993).

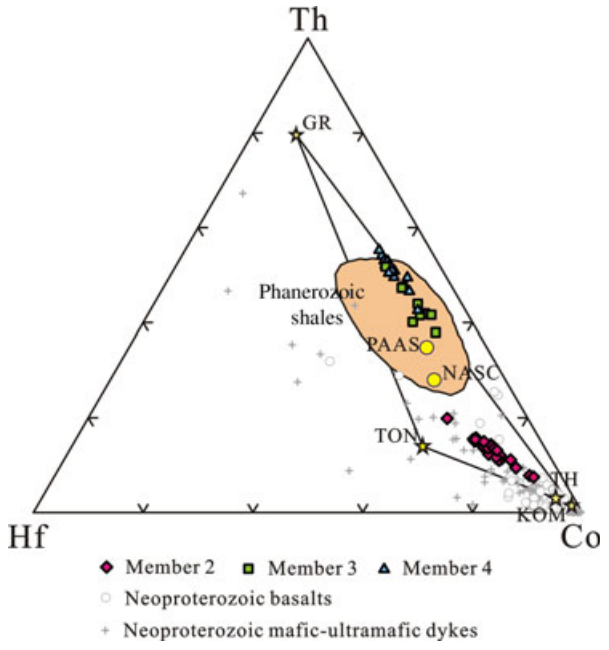

Fig. 4 Th–Hf–Co diagrams (after Jahn & Condie (1995)) for shales and carbonates of Doushantuo Formation. NASC, North American Shale Composite; PAAS, Post-Archean Australian Shale; TON, tonalite; GR, granite; TH, tholeiite; KOM, komatiite. Lines connect the four end members used in the mixing calculations of Condie (1993). Data sources for Neoproterozoic basalts and mafic–ultramafic dykes are provided in the Supplementary Information.

Granitoids and coeval mafic–ultramafic intrusions dated at ~825 Ma are distributed over a wide area of >1000 km × 700 km on the Yangtze Block (Li *et al.*, 2003) (Fig. 5) and may have been an important source of sediments to the YGA. In addition to the widely exposed Neoproterozoic mafic–ultramafic dykes, the Yiyang komatiitic basalts and Bikou basalts are found on the Yangtze Block (Li *et al.*, 2003; Wang *et al.*, 2007, 2008). There are strong geochemical similarities between the residual ~825 Ma Yiyang komatiitic basalts located about 200 km southeast of the Jiulongwan section and the sedimentary rocks of Doushantuo Member 2. The Yiyang basalts have relatively uniform Th/Zr (0.04–0.05) and Ti/Zr (51–55) ratios (Table 2) that fall in the same ranges as those for Member 2 (Th/Zr, 0.03–0.04; Ti/Zr, 46–55) (Table 2). Therefore, it is tempting to suggest that volcanics similar to the Yiyang basalts were an important source to the YGA. The current distribution of Yiyang komatiitic basalts is limited, and there is currently a large paleogeographic separation between the Yiyang komatiitic basalts and the Yangtze Gorges Basin (Fig. 5). However, it is possible that these voluminous continental flood basalts were widely distributed in the Neoproterozoic and thus could have been an important sediment source to the YGA. Nevertheless, we note that the provenance tracers simply require a strongly mafic source for the sedimentary rocks of Doushantuo Member 2 in the YGA—they do not require that the Yiyang basalts are the source.

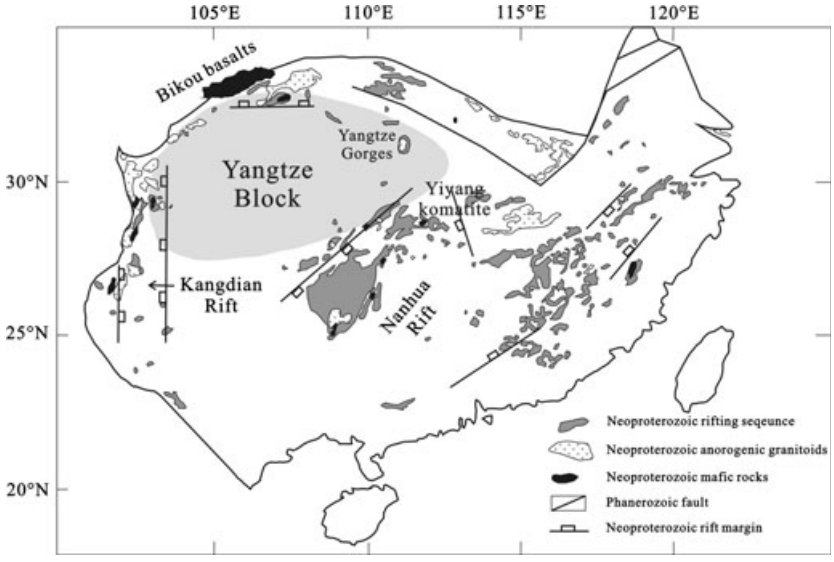

Fig. 5 Simplified map showing distribution of the Neoproterozoic mafic–ultramafic rocks on/around the Yangtze Block (after Li *et al.* (2003)).

Table 2 Comparison of MgO, Th/Zr, and Ti/Zr for sedimentary rocks of Member 2 of Doushantuo Formation and the Yiyang basaltic rocks

Sample	JLW6.6	JLW7.75	JLW10.9	JLW11.74	JLW12.25	JLW13.0	JLW13.67	JLW15.37	JLW18.38	JLW18.90	JLW20.00	JLW21.86	JLW23.85
Member	Member 2	Member 2	Member 2	Member 2	Member 2	Member 2	Member 2	Member 2	Member 2	Member 2	Member 2	Member 2	Member 2
MgO (%)	4.76	12.86	13.57	15.95	16.15	14.87	15.65	14.56	14.10	14.96	12.58	15.78	16.87
Th/Zr	0.03	0.03	0.03	0.03	0.04	0.03	0.03	0.03	0.03	0.03	0.03	0.03	0.03
Ti/Zr	50.08	47.91	49.25	53.73	49.10	47.44	49.43	45.82	52.82	50.53	49.70	51.53	49.00

Sample	JLW26.23	JLW29.70	JLW31.13	JLW37.74	JLW39.72	JLW44.00	JLW48.80	JLW54.18	JLW59.10	JLW62.78	JLW64.70	JLW68.50	JLW72.3
Member	Member 2	Member 2	Member 2	Member 2	Member 2	Member 2	Member 2	Member 2	Member 2	Member 2	Member 2	Member 2	Member 2
MgO (%)	16.72	17.59	17.87	15.58	13.58	14.41	17.09	16.06	17.29	16.38	15.29	15.11	13.85
Th/Zr	0.03	0.03	0.03	0.03	0.03	0.03	0.03	0.04	0.04	0.04	0.03	0.04	0.04
Ti/Zr	48.75	47.17	51.37	51.30	48.03	45.62	49.66	45.35	48.08	47.63	51.21	53.30	44.38

Sample	JLW76.55	JLW78.0	JLW80.4
Member	Member 2	Member 2	Member 2
MgO (%)	16.78	18.57	18.53
Th/Zr	0.04	0.04	0.04
Ti/Zr	46.43	46.38	46.46

Sample	05SC72-1	05SC72-2	05SC72-3	05SC72-4	05SC72-5	05SC72-6	05SC72-8	05SC74-2	05SC74-4	05SC74-5	05SC74-6	05SC74-7	05YY-2
Member	Yiyang	Yiyang	Yiyang	Yiyang	Yiyang	Yiyang	Yiyang	Yiyang	Yiyang	Yiyang	Yiyang	Yiyang	Yiyang
MgO (%)	4.21	17.5	12.4	10.2	10.2	11.8	14.4	13.2	13.1	14.1	11	13.4	5.9
Ti/Zr	0.05	0.04	0.04	0.04	0.04	0.04	0.04	0.04	0.04	0.04	0.04	0.04	0.05
Ti/Zr	48.75	47.17	51.37	51.30	48.03	45.62	49.66	45.35	48.08	47.63	51.21	53.30	44.38

To recap, provenance tracers in the Doushantuo Formation from the YGA indicate that sediments overlying the cap carbonate reflect two distinct sources. Member 2 was derived from surrounding Neoproterozoic mafic–ultramafic rocks, and Members 3 and 4 were likely sourced from recycled sediments with an average shale composition, and these differences are certain to have influenced the stratigraphic distribution of clay minerals within the section. Because Member 3 is carbonate-dominated, the use of detrital proxies is less straightforward. However, the carbonate inputs can be thought of as diluting the background siliciclastic flux. Further, and most importantly, there is no significant change in the detrital tracers within Member 3 or when moving into the more siliciclastic-rich Member 4. Therefore, it is reasonable to assume that there is a significant shift in the composition of the detrital flux between Members 2 and 3.

Tracing the origin of trioctahedral clays in the Yangtze Gorges area

Because saponite, a trioctahedral smectite, was found only in the cap carbonate and the mudstones of Member 2 of the Yangtze Gorges sections, Bristow *et al.* (2009) argued for a non-marine basin in the YGA during the early stages of Doushantuo deposition and that this lacustrine environment might have been hospitable to early animals. Trioctahedral smectites do commonly form in alkaline lacustrine (pH $\geq$ 9) and in isolated hypersaline marine settings. However, as mentioned earlier, these clays also commonly form during the weathering of mafic and ultramafic rocks (Smith, 1962; Meunier, 2005; Velde & Meunier, 2008). Our elemental evidence for a mafic-to-ultramafic sediment source for shales of the YGA coincides stratigraphically with the distribution of the saponite clays and is consistent with a volcanic precursor for those clays. Their up-section disappearance, in phase with a temporal shift to a very different sediment source, suggests a volcanic precursor rather than a lacustrine origin for the YGA saponite. In the Yangtze Gorges area, however, a semi-restricted shelf or lagoon in the early Doushantuo stage (Jiang *et al.*, 2011) may have favored deposition of sediments with a local provenance signature rather than a shale with an average crustal composition, which is expected for truly open-ocean shelf sediments.

We propose that the trioctahedral smectite in the YGA was produced by weathering of mafic–ultramafic rocks. Weathering of different igneous minerals can lead to differences in the resulting smectite. For example, breakdown of plagioclase and alkali feldspars commonly leads to formation of pseudomorphic dioctahedral smectite (e.g., montmorillonite), while weathering of Fe- and Mg-rich minerals (e.g., biotite or pyroxene) results in pseudomorphic replacement by trioctahedral smectite such as saponite. Weathering of acid and intermediate igneous rocks and more silicic metamorphic rocks produces a predominance of dioctahedral smectites, whereas more mafic/basaltic volcanics and volcaniclastics and metabasites tend to produce trioctahedral smectites (Chang *et al.*, 1986; Christidis & Dunham, 1997). Although weathering of mafic volcanics commonly leads to formation of a mix of trioctahedral and dioctahedral clays, similar to what are found in most alkaline lakes, there have been reported cases of formation of predominantly trioctahedral clays (See Tables S1, S2, and S3 in Supplementary Information).

Weathering of mafic volcanics involves many steps. Trioctahedral clays are the dominant products during the early stages. With increasing weathering intensity, these trioctahedral clays can destabilize, yielding dioctahedral, Fe-rich clays in the later stages (Smith, 1962; Meunier, 2005; Velde & Meunier, 2008). The key to limiting later weathering is rapid burial and high weathering rates. It is reasonable to imagine that there would have been minimal stabilization and high rates of erosion in a glacially sculpted landscape lacking any land plants.

Germanium systematics in Member 2 of the Yangtze Gorges sections also suggests a transported origin for the trioctahedral clays. Clays in Member 2 were found to have variable and very high Ge/Si ratios (>>10 μmol mol^{-1}) (Shen *et al.*, 2011). Such ratios can reflect co-deposition of detrital clays with Ge-rich, Si-poor organic complexes (Shen *et al.*, 2011). Ge-rich organic complexes are common in riverine systems (e.g., Viers *et al.*, 1997). Accordingly, high variability in Ge/Si molar ratios is likely linked to varying degrees of Ge enrichment during transport of the initial detrital clay.

Combined geochemical–sedimentological evidence also points toward continental weathering of a volcanic precursor rather than alkaline conditions in a lake (or even restricted marginal marine setting) to explain the trioctahedral clays in the YGA. The common presence of phosphatic sediments indicates active phosphogenesis at the time of deposition (Zhou *et al.*, 2007; McFadden *et al.*, 2009), and this process provides another important paleoenvironmental constraint. Incorporation of carbonate ion (CO_3^{2-}) into sedimentary carbonate fluorapatite (CFA) increases the mineral's solubility (Jahnke, 1984; Glenn *et al.*, 1994), and the concentration of phosphorous required for CFA precipitation increases exponentially as more CO_3^{2-} is substituted into the sedimentary apatite structure (Jahnke, 1984). The predominance of CO_3^{2-} expected at high pH will dramatically increase the difficulty of forming CFA under alkaline conditions. In this light, it is not surprising that there are no reports of active phosphogenesis in alkaline, saponite-forming lakes (Table S2), and so the signals for active phosphogenesis in the YGA sections point away from deposition in an alkaline lake or even under extremely alkaline restricted marine conditions. Also, most

saponite-forming alkaline lakes (85%) are associated with evaporite minerals (Table S2), evidence for which is lacking from the YGA.

Lastly, the occurrence of saponite within submembers C1 and C3 of the cap carbonate (Bristow *et al.*, 2009) also argues against an alkaline lake. C3 at the top of Member 1 and the basal carbonates of Member 2 are very similar, and so correlation between C3 in the YGA and cap carbonates distributed globally can be difficult. However, the global correlation with C1 is not in doubt. As the C1 carbonate facies shows many similarities to other caps found throughout the world in the same stratigraphic position relative to Marinoan-aged glacial deposits, including analogous C isotope trends, the marine origin for C1 in the YGA has never been questioned. Therefore, the presence of saponite within that facies argues against a lacustrine origin and is consistent with the possibility of detrital inputs into the cap-forming environment.

CONCLUSIONS

The collective data point toward a detrital origin for saponite in the lower Doushantuo Formation of the Yangtze Gorges area derived from local/regional weathering in adjacent continental areas dominated by mafic–ultramafic volcanic rocks. We propose that these arguments move the favored depositional interpretation of the lower Doushantuo and its bountiful acanthomorphic acritarch fossils, and thus potential evidence for early animal, back to a shallow marine setting, such as a shelf or lagoon. The geochemical record in the Yangtze Gorges area is entirely consistent with the marine depositional setting originally proposed based on sedimentological and basin analysis.

ACKNOWLEDGMENTS

This research is funded by the Ministry of Science and Technology of China (Grant 2011CB808805), the Natural Science Foundation of China (Grants 41172029, 41003034), and the State Key Laboratory of Continental Dynamics, Northwest University in China. Funds were provided to TWL and NJP by the U.S. National Science Foundation and the NASA Astrobiology Institute. We thank H.F. Fan and Y.X. Zhang for laboratory help. Our study also benefited from discussions with G.Q. Jiang. We are grateful for the constructive comments of G. Shields-Zhou and one anonymous reviewer.

REFERENCES

Böning P, Burmsack HJ, Bottcher ME, Schnetger B, Kriete C, Kallmeyer J, Borcher SL (2004) Geochemistry of Peruvian near-surface sediments. *Geochimica et Cosmochimica Acta* **68**, 4429–4451.

Bright CA, Cruse AM, Lyons TW, MacLeod KG, Glascock MD, Ethington RL (2009) Seawater rare-earth patterns preserved in apatite of Pennsylvanian conodonts? *Geochimica et Cosmochimica Acta* **73**, 1609–1624.

Bristow TF, Kennedy MJ, Derkowski A, Droser ML, Jiang GQ, Creaser RA (2009) Mineralogical constraints on the paleoenvironments of the Ediacaran Doushantuo Formation. *Proceedings of the National Academy of Sciences of the USA* **106**, 13190–13195.

Butterfield NJ (2011) Terminal developments in Ediacaran embryology. *Science* **334**, 1655–1656.

Cao RJ, Tang TF, Xue YS (1989) Research on Sinian strata with ore deposits in the Yangzi (Yangtze) region, China. In *Upper Precambrian of the Yangzi (Yangtze) Region, China* (ed Nanjing Institute of Geology and Palaeontology). Nanjing University Press, Nanjing, pp. 1–94.

Chang HK, Mackenzie FT, Schoonmaker J (1986) Comparisons between the Diagenesis of Dioctahedral and Trioctahedral Smectite, Brazilian Offshore Basins. *Clays and Clay Minerals* **34**, 407–423.

Christidis G, Dunham AC (1997) Compositional variations in smectites. Part II: alteration of acidic precursors, a case study from Milos island, Greece. *Clay Minerals* **32**, 253–270.

Cohen PA, Knoll AH, Kodner RB (2009) Large spinose microfossils in Ediacaran rocks as resting stages of early animals. *Proceedings of the National Academy of Sciences of the USA* **106**, 6519–6524.

Condie KC (1993) Chemical composition and evolution of the upper continental crust: contrasting results from surface samples and shales. *Chemical Geology* **104**, 1–37.

Condon D, Zhu MY, Bowring S, Wang W, Yang AH, Jin YG (2005) U-Pb ages from the neoproterozoic Doushantuo Formation, China. *Science* **308**, 95–98.

Fike DA, Grotzinger JP, Pratt LM, Summons RE (2006) Oxidation of the Ediacaran ocean. *Nature* **444**, 744–747.

Glenn CR, Föllmi KB, Riggs SR, Baturin GN, Grimm KA, Trappe J, Abed AM, Galli-Oliver C, Garrison RE, Ilyan A, Jehl C, Rohrlich V, Sadaqah RM, Schidlowski M, Sheldon RE, Siegmund H. (1994) Phosphorus and phosphorites – sedimentology and environments of formation. *Eclogae Geologicae Helvetiae* **87**, 747–788.

Hayashi K, Fujisawa H, Holland HD, Ohmoto H (1997) Geochemistry of similar to 1.9 Ga sedimentary rocks from northeastern Labrador, Canada. *Geochimica et Cosmochimica Acta* **61**, 4115–4137.

Hoffman PF, Schrag DP (2002) The snowball Earth hypothesis: testing the limits of global change. *Terra Nova* **14**, 129–155.

Huldtgren T, Cunningham JA, Yin C, Stampanoni M, Marone F, Donoghue PCJ, Bengtson S (2011) Fossilized nuclei and germination structures identify Ediacaran "animal embryos" as encysting protists. *Science* **334**, 1696–1699.

Huldtgren T, Cunningham JA, Yin C, Stampanoni M, Marone F, Donoghue PCJ, Bengtson S (2012) Response to comment on "fossilized nuclei and germination structures identify Ediacaran 'Animal embryos' as encysting protists". *Science* **335**, 1169.

Jahn BM, Condie KC (1995) Evolution of the Kaapvaal-Craton as viewed from geochemical and Sm-Nd isotopic analyses of intracratonic pelites. *Geochimica et Cosmochimica Acta* **59**, 2239–2258.

Jahnke RA (1984) The synthesis and solubility of carbonate fluorapatite. *American Journal of Science* **284**, 58–78.

Jiang GQ, Kennedy MJ, Christie-Blick N (2003) Stable isotopic evidence for methane seeps in Neoproterozoic postglacial cap carbonates. *Nature* **426**, 822–826.

Jiang G, Shi X, Zhang S, Wang Y, Xiao S (2011) Stratigraphy and paleogeography of the Ediacaran Doushantuo Formation (ca. 635–551 Ma) in South China. *Gondwana Research* **19**, 831–849.
Lev SM, McLennan SM, Hanson GN (1999) Mineralogic controls on REE mobility during black-shale diagenesis. *Journal of Sedimentary Research* **69**, 1071–1082.
Li XH, Li ZX, Ge W, Zhou H, Liu Y, Li WX, Wingate MTD (2003) Neoproterozoic granitoids in South China: crustal melting above a mantle plume at ca. 825 Ma? *Precambrian Research* **122**, 45–83.
Maynard J (1992) Chemistry of modern soils as a guide to interpreting Precambrian paleosols. *The Journal of Geology* **100**, 279–289.
McFadden KA, Huang J, Chu XL, Jiang GQ, Kaufman AJ, Zhou CM, Yuan XL, Xiao SH (2008) Pulsed oxidation and biological evolution in the Ediacaran Doushantuo Formation. *Proceedings of the National Academy of Sciences of the USA* **105**, 3197–3202.
McFadden KA, Xiao SH, Zhou CM, Kowalewski M (2009) Quantitative evaluation of the biostratigraphic distribution of acanthomorphic acritarchs in the Ediacaran Doushantuo Formation in the Yangtze Gorges area, South China. *Precambrian Research* **173**, 170–190.
McLennan SM, Taylor SR (1991) Sedimentary rocks and crustal evolution: tectonic setting and secular trends. *Journal of Geology* **99**, 1–21.
McLennan SM, Taylor SR, McCulloch MT, Maynard JB (1990) Geochemical and Nd-Sr isotopic composition of deep-sea turbidites: crustal evolution and plate tectonic associations. *Geochimica et Cosmochimica Acta* **54**, 2015–2050.
McLennan SM, Hemming S, McDanniel DK, Hanson GN (1993) Geochemical approaches to sedimentation, provenance and tectonics. In *Processes Controlling the Composition of Clastic Sediments* (eds Johnsson MJ, Basu A). Geological Society of American Special Paper 284, Boulder, CO, pp. 21–40.
Meunier A (2005) *Clays*, Springer, Berlin.
Nesbitt HW, Wilson RE (1992) Recent chemical weathering of basalts. *American Journal of Science* **292**, 740–777.
Piper DZ (1994) Seawater as the source of minor elements in black shales, phosphorites and other sedimentary-rocks. *Chemical Geology* **114**, 95–114.
Shen B, Lee CTA, Xiao SH (2011) Germanium/silica ratios in diagenetic chert nodules from the Ediacaran Doushantuo Formation, South China. *Chemical Geology* **280**, 323–335.
Smith WW (1962) Weathering of some Scottish basic igneous rocks with reference to soil formation. *Journal of Soil Science* **13**, 202–215.
Tribovillard N, Algeo TJ, Lyons TW, Riboulleau A (2006) Trace metals as paleoredox and paleoproductivity proxies: an update. *Chemical Geology* **232**, 12–32.
Velde B, Meunier A (2008) *The Origin of Clay Minerals in Soils and Weathered Rocks*, Springer, Berlin.
Vernhet E (2007) Paleobathymetric influence on the development of the late Ediacaran Yangtze platform (Hubei, Hunan, and Guizhou provinces, China). *Sedimentary Geology* **197**, 29–46.
Viers J, Dupré B, Polvé M, Schott J, Dandurand JL, Braun JJ (1997) Chemical weathering in the drainage basin of a tropical watershed (Nsimi-Zoetele site, Cameroon): comparison between organic-poor and organic-rich waters. *Chemical Geology* **140**, 181–206.
Wang XC, Li XH, Li WX, Li ZX (2007) Ca. 825 Ma komatiitic basalts in South China: first evidence for >1500°C mantle melts by a Rodinian mantle plume. *Geology* **35**, 1103–1106.
Wang XC, Li XH, Li WX, Li ZX, Liu Y, Yang YH, Liang XR, Tu XL (2008) The Bikou basalts in the northwestern Yangtze block, South China: Remnants of 820–810 Ma continental flood basalts? *Geological Society of America Bulletin* **120**, 1478–1492.
Xiao SH (2004) Neoproterozoic glaciations and the fossil record. In *The Extreme Proterozoic: Geology, Geochemistry, and Climate*. Geophysical Monograph series 146 (eds Jenkins GS, McMenamin MAS, McKey CP, Sohl L). American Geophysical Union, Washington, DC, pp. 199–214.
Xiao SH, Zhang Y, Knoll AH (1998) Three-dimensional preservation of algae and animal embryos in a Neoproterozoic phosphorite. *Nature* **391**, 553–558.
Xiao S, Knoll AH, Schiffbauer JD, Zhou C, Yuan X (2012) Comment on "fossilized nuclei and germination structures identify Ediacaran'animal embryos' as encysting protists". *Science* **335**, 1169.
Yin LM, Zhu MY, Knoll AH, Yuan XL, Zhang JM, Hu J (2007) Doushantuo embryos preserved inside diapause egg cysts. *Nature* **446**, 661–663.
Zhou CM, Xie GW, McFadden K, Xiao SH, Yuan XL (2007) The diversification and extinction of Doushantuo-Pertatataka acritarchs in South China: causes and biostratigraphic significance. *Geological Journal* **42**, 229–262.
Ziemniak SE, Jones ME, Combs KES (1993) Solubility behavior of titanium (iv) oxide in alkaline media at elevated-temperatures. *Journal of Solution Chemistry* **22**, 601–623.

SUPPORTING INFORMATION

Additional Supporting Information may be found in the online version of this article:

Table S1. Occurrences of trioctahedral smectite in modern and ancient marine sediments.

Table S2. Occurrences of trioctahedral smectite in modern and ancient lacustrine sediments.

Table S3. Occurrences of trioctahedral smectite in soils and mafic rocks.